# Optimal topology for parallel discrete-event simulations

Yup Kim, Jung-Hwa Kim, and Soon-Hyung Yook*
*Department of Physics and Research Institute for Basic Sciences, Kyung Hee University, Seoul 130-701, Korea*
(Received 26 December 2010; published 19 May 2011)

The effect of shortcuts on the task completion landscape in parallel discrete-event simulation (PDES) is investigated. The morphology of the task completion landscape in PDES is known to be described well by the Langevin-type equation for nonequillibrium interface growth phenomena, such as the Kardar-Parisi-Zhang equation. From the numerical simulations, we find that the root-mean-squared fluctuation of task completion landscape, $W(t,N)$, scales as $W(t\to\infty,N)\sim N$ when the number of shortcuts, $\ell$, is finite. Here $N$ is the number of nodes. This behavior can be understood from the mean-field type argument with effective defects when $\ell$ is finite. We also study the behavior of $W(t,N)$ when $\ell$ increases as $N$ increases and provide a criterion to design an optimal topology to achieve a better synchronizability in PDES.

DOI: 10.1103/PhysRevE.83.056115 PACS number(s): 89.75.Hc, 64.60.aq, 68.35.Ct, 89.20.Ff

## I. INTRODUCTION

During the past few years, many studies of complex networks have focused on the dynamic processes taking place on given network topologies. Among such studies, synchronization phenomena observed in various natural and artificial systems have been attracted many researchers in various fields ranging from physics to biology and sociology [1–3]. On networks, each individual element represented by a node adjust its state through the interactions with its local neighbors. Thus understanding the effect of the interaction topology between individuals on the synchronization is very important to uncover various complex behaviors in such systems. Especially, due to its theoretical and practical importance, the efficient method to find an optimal topology which gives the best synchronizability has been widely investigated. Applications of the corresponding models range from physics [3], biology [4], distributed computing [2], and consensus formation [5]. In those systems the local state variables are assumed to have finite number of possible values. As the system evolves in time, the values of the local state variables change synchronously or asynchronously depending on the dynamics of the system.

Recently, the synchronization of the parallel discrete-event simulations (PDES) has been studied on small-world networks [2]. Examples of PDES applications include dynamic channel allocation in cell phone networks, models of the disease spreading, battle-field simulation, and dynamic phenomena in highly anisotropic magnetic systems [2]. Here the discrete events are call arrivals, infections, troop movements, and changes of the orientation of the local magnetic moments, respectively. As the number of processing elements (PEs) increases, the scalability in the synchronization becomes important. In the PDES scheme, the scalar field $h_i$ is assigned to each node (or site) $i$ which describes the time it takes to finish a job or the amount of the work that has to be accomplished. If we interpret $h_i$ as the height of interface in the nonequilibrium roughening phenomena, then the synchronization can be analyzed by investigating the average roughness of the interface. Based on this interpretation, the dynamics and fluctuations of task completion landscape, $\{h_i\}$, [2,6] have been approximated by the Edwards-Wilkinson (EW) [7] or Kardar-Parisi-Zhang (KPZ) [8] equations for dynamic roughening phenomena. Like many other synchronization problems, the complex structure of the underlying interaction networks are known to strongly affect the fluctuations of task completion landscape even for a linear model which belongs to EW universality class [9]. More recently, the morphological properties of innovation spreading were investigated using a simple stochastic model [5]. In this model the interplay between the underlying topology and avalanche become very crucial for the morphological transition. The dynamic rule of the innovation spreading model is very close to that of restricted solid-on-solid (RSOS) model with avalanches [10]. When the noise is not quenched, RSOS model with avalanche belongs to the KPZ universality class [11]. Therefore, it is theoretically also interesting to study the effect of the underlying topology on the morphological transition of the model belongs to the KPZ universality class.

## II. CONTINUUM EQUATION

Using the coarse-graining procedure, the time evolution of state variable $h_i$ for each PE was shown to be well approximated by the KPZ equation when there is synchronization/communication between neighboring PEs [2,6],

$$\frac{\partial h(\mathbf{x},t)}{\partial t}=\nu\nabla^2 h+\lambda\,(\nabla h)^2+\eta(\mathbf{x},t). \tag{1}$$

Here $\eta(\mathbf{x},t)$ is Gaussian white noise that satisfies the relation

$$\begin{aligned}\langle\eta(\mathbf{x},t)\rangle&=0,\\ \left\langle\eta(\mathbf{x},t)\eta(\mathbf{x}',t')\right\rangle&=2D\delta^d(\mathbf{x}-\mathbf{x}')\delta(t-t').\end{aligned} \tag{2}$$

We already showed that the diversity of technological level also can be described by the concepts developed in the studies on kinetic surface roughening [11]. In this study we use the same method to analyze the synchronizability in PDES scheme as suggested in Ref. [2]. The synchronizability in PDES scheme can be measured by the root-mean-square of the task completion landscape for $N$ PEs, which corresponds to the interface width, $W(t,N)$, defined as

$$W(t,N)=\left(\frac{1}{N}\sum_{i=1}^{N}[h_i(t)-\bar{h}(t)]^2\right)^{\frac{1}{2}}. \tag{3}$$

*syook@khu.ac.kr

 ©2011 American Physical Society

Here $\bar{h}(t)$ stands for the average task completion level at time $t$,

$$\bar{h}(t) = \frac{1}{N}\sum_{i=1}^{N} h_i(t). \tag{4}$$

$W(N,t)$ normally satisfies the finite-size scaling ansatz [12,13]

$$W(t,N) \sim N^{\alpha} f\left(\frac{t}{N^{z}}\right), \tag{5}$$

where the function $f(x)$ scales as $f(x) \sim x^{\beta}$ for $x \ll 1$ and $f(x) \to$ const. for $x \gg 1$, and the dynamic exponent $z$ satisfies the relation $z = \alpha/\beta$.

## III. MODEL AND UNDERLYING TOPOLOGY

In order to study the interplay between synchronization and interaction topology in the PDES scheme, we consider Sneppen's B model [10] without quenched noise because the model belongs to the KPZ universality class. The model is originally defined on a one-dimensional ($1d$) ring with periodic boundary condition as follows: (i) Place $N$ PEs at each node (or site). (ii) Starting from an initially flat task completion landscape ($h_i(t=0) = 0, \forall i$), select a node $i$ at random. (iii) Increase the task completion level of $i$ by unity, i.e., $h_i \to h_i + 1$. (iv) Then the neighboring sites are adjusted upward by unity until all slopes satisfy $|h_i - h_{i-1}| \leqslant 1$, for all $i$ (restricted solid-on-solid (RSOS) condition).

As shown in Ref. [5] the underlying topology crucially affects the diversity of technological level, which corresponds to the synchronizability in PDES. Moreover, the internetworked structures of computers are known to be characterized by the small-world networks [14–16] in which the diameter of network scales as $\ln N$. Thus, it is natural to investigate the synchronizability in PDES on small-world networks. Therefore, the study on the interplay between underlying topology and synchronizability in PDES is very important not only theoretically but also practically. For this purpose, we extend the underlying topology to small-world networks by randomly or regularly adding $\ell$ shortcuts to the $1d$ structure [15,16] and study the dependence of $W(t,N)$ on $\ell$.

## IV. NUMERICAL RESULTS

### A. $W(t,N)$ for finite number of shortcuts

When there is no shortcut, the model belongs to the KPZ universality class, whose scaling exponents are known as $\beta = 1/3$ and $\alpha = 1/2$ on a $1d$ substrate. In Fig. 1 we display $W(t,N)$ when we randomly add $\ell$ shortcuts to the $1d$ structure [(a) $\ell = 1$ and (b) $\ell = 10$, respectively]. For both cases, we find that $\beta \approx 1/3$ when $t < 100$. Then $\beta$ increases abruptly and we obtain $\beta \approx 0.9$ for $\ell = 1$ and $\beta \approx 0.7$ for $\ell = 10$. This indicates that when $t < 100$ the correlation length is much smaller than the average distance between two neighboring shortcuts. Therefore, the morphological property of task completion landscape is simply the same with that on $1d$ substrate. As a result the $\beta$ for early time is identical with that of KPZ value $\beta = 1/3$. However, if $t$ becomes large (in these examples, $t > 100$) then the effect of shortcuts is turned on. As shown in the data in Figs. 1(a) and 1(b), the value of $\beta$ for relatively large

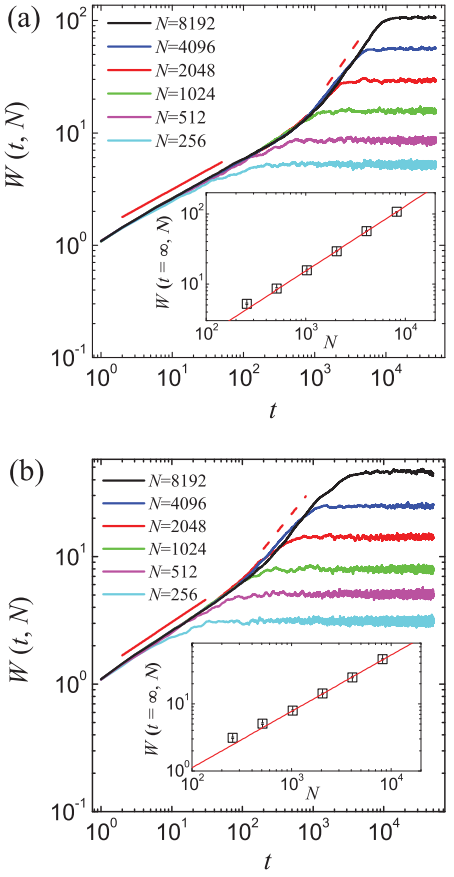


FIG. 1. (Color online) Plot of $W(t,N)$ when (a) $\ell = 1$ and (b) $\ell = 10$. $N$ varies from 256 (bottom) to 8192 (top). Solid lines represent (a) $\beta \approx 0.35$ and (b) $\beta \approx 0.36$. The dashed lines correspond to (a) $\beta \approx 0.9$ and (b) $\beta \approx 0.7$. Insets show the $W(N)$ when the system is in the steady state. The lines represent the relation $W(N) \sim N^{\alpha}$. From the data we obtain (a) $\alpha = 0.92$ and (b) $\alpha = 0.84$.

$t$ increases as $N$ increases. Thus we expect that $\beta$ for large $t$ and $N$ eventually approaches to 1. We also display the behavior of $W(t \to \infty, N)$ for $\ell = 1$ and $\ell = 10$ in each inset. Using Eq. (5) we obtain $\alpha \approx 0.92$ for $\ell = 1$ and $\alpha \approx 0.84$ for $\ell = 10$. These value of $\beta$'s and $\alpha$'s are quite close to $\beta = \alpha = 1$ which are expected when there is a strong point defect [17,18].

### B. Morphology and height-height correlation function

For a more systematic approach, we place shortcuts with equal spacing as shown schematically in Fig. 2(a). Thus, the addition of $\ell$ shortcuts divides the $1d$ lattice of node $N$ into $2\ell$ segments and there are $N/2\ell$ nodes in each segment. To investigate whether the shortcuts induce effective defects, we first take snapshots of the morphologies for $N = 8192$. Figures 2(b) and 2(c) show typical examples of morphologies for $\ell = 1$ and $\ell = 3$ when $W(t,N)$ is in a steady state. In these examples, the pairs of nodes connected by shortcuts are $(0, N/2)$ for $\ell = 1$ and $(0, N/2)$, $(N/6, 4N/6)$, and $(2N/6, 5N/6)$ for $\ell = 3$. In Figs. 2(b) and 2(c) the locations of shortcuts are depicted by down/up triangles. The morphology clearly shows that the $h$'s at the nodes connected to a shortcut grow much faster than those at the nodes without shortcuts. As a result, the nodes at the midpoints between two neighboring

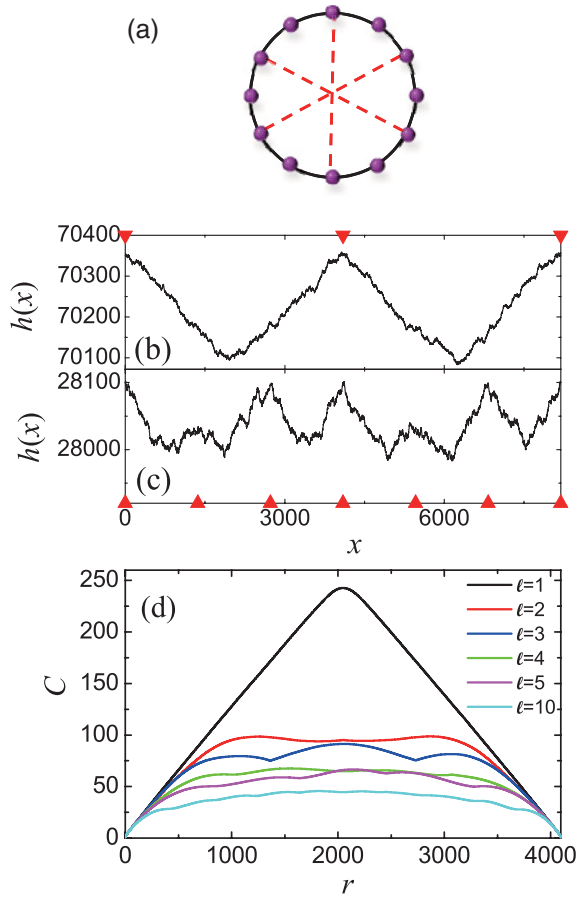


FIG. 2. (Color online) (a) Schematic diagram for the shortcut locations for $\ell = 3$. The solid line denotes $1d$ underlying structure. The dashed lines represent the additional shortcut. In this example, $\ell = 3$. The $\ell$ shortcuts divide the $1d$ ring into $2\ell$ segments. Each segment contains $N/2\ell$ nodes. Morphologies when the system is in a steady state for (b) $\ell = 1$ and (c) $\ell = 3$. Down (up) triangles represents the location of shortcuts for $\ell = 1$ ($\ell = 3$). (d) Plot of $C(r)$ for various $\ell$ when $N = 8192$. Top curve corresponds to $\ell = 1$ and bottom curve represents the data for $\ell = 10$.

shortcuts play a role of effective defects at which the growth of $h$ is slow compared to those with shortcuts. For a more detailed analysis we measure the height-height correlation function [see Fig. 2(d)]. The height-height correlation function between two points separated by a distance $r$, $C(r)$, is defined as

$$C(x_0,r,t) = \langle |h(x_0 + r,t) - h(x_0,t)| \rangle . \tag{6}$$

Here we fix $x_0 = 0$ and the $\langle \cdots \rangle$ represents the average over realizations. The data in Fig. 2(d) clearly show that $C(r)$ increases until $r = N/4\ell$ which corresponds to the half of the distance between two nearest shortcuts. This coincides with the location of the nearest effective defects from $x_0$. Then $C(r)$ remains at almost a constant value for $N/4\ell < r < (N/2) - (N/4\ell)$. As we further increase $r$, $C(r)$ decreases and finally becomes zero at $r = N/2$. This result indicates that $C(r)$ increases until $r$ reaches the effective defect located at $r = N/4\ell$. However, due to the defect, $C(r)$ cannot further increase for $N/4\ell < r < (N/2) - (N/4\ell)$.

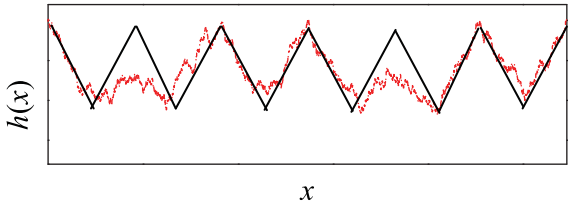


FIG. 3. (Color online) Red (gray) dashed line represents the morphology for $\ell = 3$. Black lines denote the approximated morphology by successive triangles.

### C. Mean-field argument for $W(t \to \infty, N; \ell)$ when $\ell$ is fixed

When the number of shortcuts is fixed or $\ell/N \to 0$ as $N \to \infty$, we expect $W(t \to \infty, N) \simeq N$ as in Fig. 1. We now want to explain the behavior of $W(t \to \infty, N) \simeq N$ by a mean-field type argument. Based on the measurement of $W(t, N)$ for fixed $\ell$ and morphology, we find that the shortcuts induce defects. Due to the induced defects, the morphology can be approximated by successive triangles as shown in Fig. 3(a). As for the measurement in Fig. 2, we assume that the distances between two nearest shortcuts are same. The length of the base line of each triangle is given by the distance between the nearest shortcuts [in Figs. 2(b) and 2(c), the distance between the nearest triangles]. We also assume that the fluctuation in the heights of triangles can be ignored. Based on these assumptions we can approximate morphology by the triangles with the same base line length and height. Without loss of generality the slope of triangle is set to be unity. Then the $\langle h \rangle$ and $\langle h^2 \rangle$ can be easily obtained as

$$\langle h \rangle = \frac{1}{N} \sum_{i=1}^{N} h_i = \frac{1}{N} \left( 4\ell \sum_{i=1}^{N/4\ell} i \right) \tag{7}$$

and

$$\langle h^2 \rangle = \frac{1}{N} \left( 4\ell \sum_{i=1}^{N/4\ell} i^2 \right), \tag{8}$$

respectively. From Eqs. (3), (7), and (8), $W(t \to \infty, N; \ell)$ becomes

$$W = \sqrt{\frac{1}{12}} \left( \frac{N^2}{16\ell^2} - 1 \right)^{1/2} . \tag{9}$$

Thus, when $\ell$ is fixed, $W(t \to \infty, N; \ell)$ scales as $W \sim N$ which shows a good agreement with the results obtained from Fig. 1. Note that Eq. (9) is valid only for $4\ell \leqslant N$. Since there are $N/2\ell$ nodes between two neighboring shortcuts, this condition implies that there should be at least one node between two neighboring shortcuts which plays a role of effective defect.

### D. $W(t \to \infty, N; \ell)$ when $N$ is fixed

More recently, EW equation on SW networks was studied and was shown to have anomalous scaling with $\ell$ when $N$ is fixed [6]. Using the analytic arguments and numerical simulations, they showed that $W(t \to \infty, N; \ell)$ scales as $W(t \to \infty, N; \ell) \sim \ell^{-1/2}$ when $\ell \leqslant N$. Thus, it is natural to ask how the nonlinear term in Eq. (1) affects the anomalous scaling with $\ell$ and the synchronizability in PDES. In Fig. 4 we

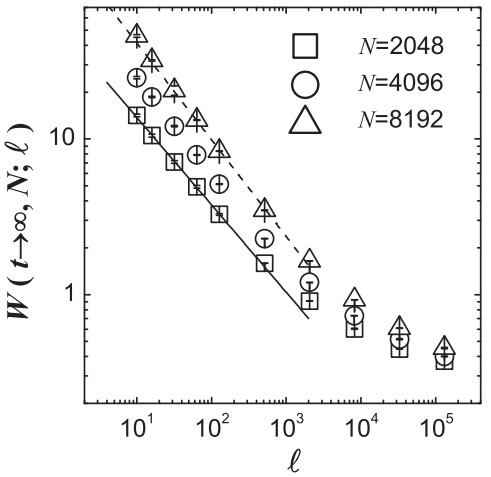


FIG. 4. Plot of $W(t \to \infty, N; \ell)$ in a steady state when $N$ is fixed. The solid line represents the relation $W \sim \ell^{-0.56}$ and the dashed line denotes $W \sim \ell^{-0.62}$.

show the behavior of $W(t \to \infty, N; \ell)$ of Sneppen's B model without quenched noise when $N$ is fixed to be $N = 2048$, 4096, and 8192. Here we add $\ell$ shortcuts at random. As shown in Fig. 4, $W(t \to \infty, N; \ell)$ also satisfies the power law

$$W(t \to \infty, N; \ell) \sim \ell^{-\delta}, \tag{10}$$

for $\ell \leqslant N$. Using the least-squares fit of the data to Eq. (10) we obtain $\delta \simeq 0.56$ for $N = 2048$ and $\delta \simeq 0.62$ for $N = 8192$ when $\ell < N$. This clearly shows that $\delta$ increases as we increase $N$. Moreover, the obtained value of $\delta$ is larger than that for EW equation. This result indicates that the nonlinear term caused by the communication between neighboring PEs enhances the synchronizability. Since the possible maximum value of $\ell$ is $N(N-1)/2 - N$, it is also important to investigate the behavior of $W(t \to \infty, N; \ell)$ when $\ell > N$. Even when $\ell$ is slightly larger than $N$, we find that $W(t \to \infty, N; \ell)$ significantly deviates from the power law. As $\ell$ increases further, the underlying topology becomes identical to fully connected network. Thus, we expect that $W(t \to \infty, N; \ell)$ would converge to some constant value which is close to zero due to the RSOS condition.

### E. $W(t \to \infty, N; \ell)$ when $\ell \propto N^{\kappa}$

As shown in Secs. IV A and IV D, when $\ell$ is finite, the shortcuts induce effective defects and $W(t \to \infty, N; \ell)$ starts to deviate from a power law (10) when $\ell \sim N$. This implies that when $\ell \propto N^{\kappa}$ with $\kappa < 1$ the shortcuts produce effective defects and $W(t \to \infty, N; \ell)$ diverges in the limit $N \to \infty$. Therefore, investigating the detailed behavior of $W(t \to \infty, N; \ell)$ when $\kappa \geqslant 1$ has practical importance to find a criterion for an optimal topology in synchronization.

In Fig. 5, we display $W(t \to \infty, N; \ell)$'s for randomly connected $\ell$ shortcuts when $\kappa = 1$. This implies that the average number of shortcuts per node remains finite in the limit $N \to \infty$. As shown in the inset of Fig. 5(a),

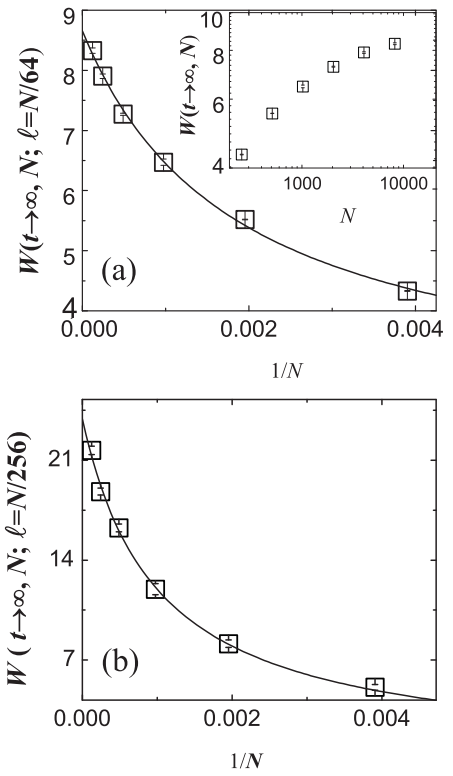


FIG. 5. Plot of $W(t, N; \ell)$ when (a) $\ell = N/64$ and (b) $\ell = N/256$. The solid line represents the extrapolation of the data. The lines intersect the vertical axes at (a) $W = 8.7$ and (b) $W = 23.9$, respectively.

we find that the increment in $W(t \to \infty, N; \ell)$ decreases as we increase $N$. In Figs. 5(a) and 5(b) we plot $W(t \to \infty, N; \ell)$ against $1/N$ for $\ell = N/64$ and $\ell = N/256$. From the extrapolations of the data we find $W(t \to \infty, N \to \infty; \ell = N/64) \simeq 8.7$ and $W(t \to \infty, N \to \infty; \ell = N/256) \simeq 23.9$,

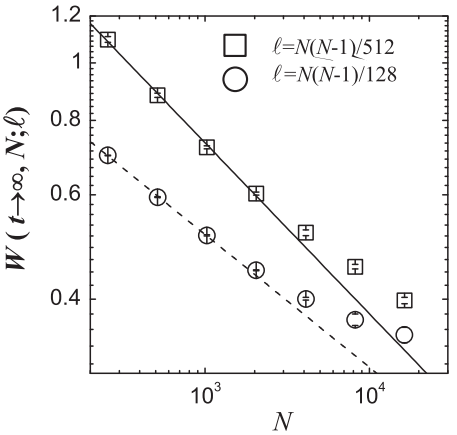


FIG. 6. Plot of $W(t \to \infty, N; \ell)$ against $N$. The squares represent the data for $\ell = N(N-1)/512$ and circles denote the data for $\ell = N(N-1)/128$. The solid line represents the relation $W(t \to \infty, N) \sim N^{-0.27}$ and the dashed line displays the relation $W(t \to \infty, N) \sim N^{-0.22}$. For $N > \ell$, $W(t \to \infty, N)$ deviates from the power law for both $\ell$'s.

which are very close to the mean-field expectations based on Eq. (9) [$W(t \to \infty, N \to \infty; \ell = N/64) \simeq 4.61$ and $W(t \to \infty, N \to \infty; \ell = N/256) \simeq 18.47$]. This clearly shows that the roughness of the task completion landscape does not diverge when $\ell \propto N$ in the limit $N \to \infty$.

In Fig. 6 we also measure the $W(t \to \infty, N; \ell)$ when $\ell$ increases as $\ell \propto N(N-1)/2$ which corresponds to the case $\kappa = 2$ for $N \gg 1$. The $\ell$ shortcuts are randomly added to the $1d$ structure. As shown in Fig. 6, we find that $W(t \to \infty, N; \ell)$ scales as $W(t \to \infty, N; \ell) \sim N^{\alpha}$ for $N > \ell$. From the least-squares fit of the data to the power law, we obtain $\alpha \simeq -0.27$ for $\ell = N(N-1)/512$. However, we find that $\alpha$ increases as we increase $\ell$. In this example, we obtain $\alpha \simeq -0.22$ for $\ell = N(N-1)/124$ when $N > \ell$. Thus, the obtained values of $\alpha$ when $\ell \propto N(N-1)$ are not universal even though it follows the power law when $N > \ell$. For $N < \ell$, $W(t \to \infty, N; \ell)$ significantly deviates from the power law. Note that when $\kappa > 1$, $\ell$ increases much faster than $N$ and the underlying topology would be identical with the fully connected network in the limit $N \to \infty$. Therefore, for $\ell > N$ we expect that $W(t \to \infty, N; \ell)$ will converge to a value which is close to zero as in Fig. 4. Thus, for the most optimal topology to achieve the best synchronizability in PDES, $\kappa$ should be larger than 1.

However, as shown in Figs. 4 and 6 the differences in $W(t \to \infty, N; \ell)$ for $\ell > N$ are relatively small compared to that for $\ell < N$. This implies that the effect of additional shortcuts for $\ell > N$ becomes less drastic than that for $\ell < N$. Moreover, the data in Fig. 5 indicate that the number of additional shortcut should be at least proportional to $N$ to obtain nondiverging $W(t \to \infty, N \to \infty; \ell)$. Thus, the condition, $\ell \simeq \mathcal{O}(N)$, would play a role of the criterion for an optimal shortcut number to achieve better synchronizability from the practical point of view.

## V. SUMMARY

In this study, we investigate the effect of the underlying topology to the synchronizability in PDES. Since the task completion landscape is known to be well described by the KPZ equation, we use the Sneppen's B model without quenched noise which belongs to the KPZ universality class. To generate the small-world topology, we randomly or regularly add $\ell$ shortcuts to the $1d$ lattice. From the numerical simulations we find that the shortcuts produce some effective defects when $\ell$ is finite. Using the mean-field like argument with equally spaced shortcuts, we derive the correct scaling behavior of $W(t, N; \ell)$ for fixed $\ell$. When $N$ is fixed, we find that $W(t \to \infty, N; \ell)$ scales as $W(t \to \infty, N; \ell) \sim \ell^{-\delta}$ for $\ell < N$ like in EW equation. However, we find that the obtained $\delta$ is larger than that for EW equation, which indicates that the nonlinear term caused by communication between neighboring PEs enhances the synchronizability. We also investigate the behavior of $W(t \to \infty, N; \ell)$ when $\ell \propto N^{\kappa}$ and find that $W(t \to \infty, N; \ell)$ does not diverge for $\kappa \geqslant 1$. Based on our measurements of $W(t \to \infty, N; \ell)$, we find that the most optimal topology in PDES can be obtained when $\kappa > 1$ in the limit $N \to \infty$. However, as a practical condition for $\ell$ to obtain non diverging $W(t, N; \ell)$, we find that there should be at least one shortcut per node. We expect that our criterion for synchronizability in PDES can be easily applied to the designing of networks for various distributed computing systems.

## ACKNOWLEDGMENTS

This work was supported by Basic Science Research Program through the National Research Foundation of Korea (NRF) funded by the Ministry of Education, Science and Technology (2010-0021586 and 2009-0073939).

[1] A. Pikovsky, M. Rosenblum, and J. Kruths, *Synchronization: A Universal Concept in Nonlinear Science* (Cambridge University Press, Cambridge, 2010).
[2] G. Korniss, M. A. Novotny, H. Guclu, Z. Toroczkai, and P. A. Rikvold, Science **299**, 677 (2003).
[3] Y. Kim, Y. Ko, and S. -H. Yook, Phys. Rev. E **81**, 011139 (2010).
[4] L. Glass, Nature **410**, 277 (2001).
[5] Y. Kim, B. Han, and S.-H. Yook, Phys. Rev. E **82**, 046110 (2010).
[6] B. Kozma, M. B. Hastings, and G. Korniss, Phys. Rev. Lett. **92**, 108701 (2004).
[7] S. F. Edwards and D. R. Wilkinson, Proc. R. Soc. London A **381**, 17 (1982).
[8] M. Kardar, G. Parisi, and Y.-C. Zhang, Phys. Rev. Lett. **56**, 889 (1986).
[9] A. L. Pastorey Piontti, P. A. Macri, and L. A. Braunstein, Phys. Rev. E **76**, 046117 (2007).
[10] K. Sneppen, Phys. Rev. Lett. **69**, 3539 (1992).
[11] A.-L. Barabási and H. E. Stanely, *Fractal Concepts in Surface Growth* (Cambridge University Press, Cambridge, 1995).
[12] F. Family and T. Vicsek, J. Phys. A: Math. Gen. **18**, L75 (1985).
[13] In order to extend the analysis to the data obtained from networks, we use the number of nodes, $N$, instead of linear dimension $L$.
[14] S. H. Yook, H. Jeong, and A.-L. Barabási, Proc. Nat. Acad. Sci. U.S.A. **99**, 13382 (2002).
[15] D. J. Watts and S. H. Strogatz, Nature **393**, 440 (1998).
[16] M. E. J. Newman and D. J. Watts, Phys. Rev. E **60**, 7332 (1999).
[17] F. Slanina and M. Kotrla, Physica A **256**, 1 (1998).
[18] S. H. Yoon and Y. Kim, J. Phys. Soc. Jpn. **75**, 104003 (2006).